Nanoscale Advances

ROYAL SOCIETY OF CHEMISTRY

PAPER

View Article Online
View Journal | View Issue

Cite this: *Nanoscale Adv.*, 2025, **7**, 1814

$MgO@SiO_2$ nanocapsules: a controlled magnesium ion release system for targeted inhibition of osteoarthritis progression†

Na Liu,[a] Fangchao Jiang,[b] Zhizi Feng,[b] Sen Mei,[a] Yingna Cui,[c] Yu Zheng,[a] Wei Yang,[b] Benjie Wang,[a] Weizhong Zhang,[b] Jin Xie *[b] and Nan Zhang *[a]

Osteoarthritis (OA) is a chronic joint disease characterized by degenerative changes in articular cartilage and chronic inflammation. Recent studies suggest that intra-articular (i.a.) injection of magnesium salts holds promise as a therapeutic approach for OA. However, the rapid diffusion of magnesium ions limits their efficacy, resulting in a short duration of action. To overcome this limitation, we developed a nanoparticle delivery system using $MgO@SiO_2$ core/shell nanoparticles, designed as a depot for the controlled release of magnesium ions. Electron microscopy confirmed the formation of the core/shell structure with silica shells of varying thickness. Release studies demonstrated that the silica coating effectively slows nanoparticle degradation, extending magnesium release to over 72 hours. In a rabbit OA model, i.a. injection of these nanocapsules significantly mitigated the pathological progression of OA within four weeks without inducing systemic toxicity. Immunohistochemical analysis further revealed that $MgO@SiO_2$ nanocapsules alleviate the inflammatory response in OA cartilage by inhibiting the NF-κB/p65 signaling pathway. In summary, this study confirms the potential of intra-articular magnesium supplementation as a therapeutic option for OA and introduces a novel approach to enhance the delivery and efficacy of magnesium ions in OA treatment, addressing a relatively underexplored area in the field.

Received 1st November 2024
Accepted 17th January 2025

DOI: 10.1039/d4na00900b

rsc.li/nanoscale-advances

1 Introduction

Osteoarthritis (OA) is a common and disabling disease that not only causes significant pain and economic burden to patients, but also has a profound impact on society as a whole.[1,2] It is characterized by an inflammatory environment and articular cartilage damage, leading to more severe synovial edema, osteophytes and subchondral bone sclerosis, which cause joint dysfunction, pain, stiffness, functional limitations and loss of valued activities.[3] The pathogenesis of OA remains unclear because it is not caused by a single factor but rather results from a combination of multiple factors. Clinically available interventions are limited to palliative care to relieve symptoms, with total joint replacement as an option for advanced symptoms or significant dysfunction.[4] Currently, the commonly used drugs for treating OA include selective COX-2 enzyme inhibitors, non-steroidal anti-inflammatory drugs (NSAIDs), glucocorticoids, viscosupplements, and other traditional medications. Direct intra-articular injection of these drugs is widely practiced due to its advantage of bypassing the poor joint bioavailability associated with systemic administration. However, rapid drug clearance from the joint remains a significant limitation, reducing the efficacy of most therapeutic molecules. More importantly, while intra-articular drug injections can alleviate inflammatory symptoms and slow disease progression, they cannot reverse the course of the disease or provide a cure for OA. Therefore, continued efforts to develop new treatment approaches for OA are critical.

There has been growing interest in the role of Mg^{2+} in the pathophysiological changes of osteoarthritis (OA) in the last decade.[5,6] Mg^{2+} has been shown to promote the proliferation and differentiation of ATDC5 cells while inhibiting their mineralization.[7] It also enhances the adherence of mesenchymal stem cells (MSCs) through integrins, thereby supporting the early synthesis of the cartilage matrix.[8] In addition to its direct effect on chondrocyte metabolism, elevated magnesium levels influence the efficacy of growth factors during chondrogenesis.[9] In our previous study, a significant presence of chondrocytes was observed around the degradation products of magnesium-based implants.[10] Conversely, magnesium deficiency is associated with inflammation, cartilage damage, defective chondrocyte biosynthesis, aberrant calcification, and reduced analgesic efficacy.[11] Mg^{2+} supplements, such as $MgCl_2$ and $MgSO_4$, have been administered orally or intra-articularly to

[a]*Affiliated Xinhua Hospital of Dalian University, Dalian, Liaoning, 116000, China. E-mail: zhn1979-08@163.com*

[b]*Department of Chemistry of University of Georgia, Athens, Georgia, 30602, USA. E-mail: jinxie@uga.edu*

[c]*Department of Chemistry of Dalian University, Dalian, Liaoning, 116000, China*

† Electronic supplementary information (ESI) available. See DOI: https://doi.org/10.1039/d4na00900b

treat OA in clinical settings. Recent studies have shown that intra-articular injection of $MgCl_2$ can inhibit the NF-κB pathway, reduce the expression of inflammatory factors, and alleviate the inflammatory response in OA cartilage.[12] However, Mg salts are rapidly cleared from the injection site and lose their therapeutic effect.[13] Increasing the injection dose easily exceeds the toxicity threshold of the treatment window, making the treatment less effective and even causing toxic events. There is an urgent need for delivery methods that allow for sustained release of Mg^{2+} in the joint space.

To deliver Mg^{2+} into the joint cavity, it is essential to identify a suitable carrier. While metallic magnesium contains the highest Mg content, its high reactivity poses significant biosafety concerns, making it unsuitable for clinical applications. Additionally, although $MgCO_3$ and $Mg(OH)_2$ are more stable, their magnesium content is lower than magnesium oxide (MgO) content. More importantly, MgO can be prepared into nano form, demonstrating unique advantageous properties, including a large surface area-to-volume ratio, high chemical stability, and non-toxicity.[14] A large number of studies have reported that MgO NPs have been used in various biomedical applications, such as cancer treatment, antibacterial activity, antioxidant effect, and anti-aging therapy.[15–17] Recently, MgO nanoparticles (NPs) have been incorporated into a water-soluble phosphocreatine-functionalized chitosan solution to form a hydrogel, which has shown potential for promoting bone regeneration.[18] Additionally, MgO@PLGA nanocapsules, prepared using polylactic–glycolic acid (PLGA) copolymer microspheres loaded with MgO NPs, have been reported as a potential treatment for OA.[19] More importantly, the adjustable particle size of MgO NPs makes them well-suited for intra-articular administration. Our previous study demonstrated that MgO NPs can prolong the release time of Mg^{2+} by adjusting the particle size, and can effectively alleviate cartilage injury and degeneration associated with OA.[20] However, we also found that the release duration of MgO NPs does not align with the typical clinical schedule for intra-articular injections, which are often administered weekly.[21] Therefore, a delivery system that provides a more sustained release of magnesium is needed.

To address this need, we developed and evaluated a nanocapsule technology. Specifically, we synthesized $MgO@SiO_2$ core/shell nanoparticles. The silica coating prevents the rapid degradation of the magnesium core in aqueous environments, enabling gradual nanocrystal degradation and controlled magnesium release. This technology allows for the intra-articular injection of a high magnesium dose, providing effective OA treatment without causing local or systemic toxicity. In this study, we focused on evaluating the *in vitro* release profile and toxicity of the nanocapsules. Furthermore, their protective effects against OA-related cartilage destruction and their potential mechanism for reducing inflammation were assessed using a rabbit knee OA model.

2 Materials and methods

2.1 Materials and preparation of samples

The synthesis of MgO NPs was based on a previously reported protocol with minor modifications.[22] Briefly, 2 mmol (0.445 g) of magnesium 2,4-pentanedionate hydrate ($Mg(acac)_2 \cdot 2H_2O$, Sigma-Aldrich, USA) was used as the precursor and added into a three-necked flask (100 mL) containing 16 mmol (4.288 g) of oleylamine (Sigma-Aldrich, USA), 4 mmol (1.128 g) of oleic acid (Sigma-Aldrich, USA), and 20 mmol (5.05 g) of 1-octadecene (Sigma-Aldrich, USA). The mixture was heated to 150 °C under an argon atmosphere and reacted for 15 min. After the solution turned light yellow, the temperature was raised to 300 °C and the reaction continued for an additional 60 min. The reaction mixture was then cooled to room temperature, and the MgO NPs were precipitated by adding an excess of ethanol and glycerol (3 : 1). The process was repeated three times to remove excess 1-octadecene, unreacted precursors and surfactants.

To slow the degradation of the as-synthesized MgO NPs, the nanoparticles were coated with a silica layer using the Stöber method. Briefly, the MgO NPs were dispersed in a mixture of ethanol and 0.2 mL ammonia (28%), and mixed at room temperature and added dropwise (10 s per drop) with 90 μL and 180 μL of tetraethyl orthosilicate (TEOS, Sigma-Aldrich, USA) with continuous stirring for 24 h to obtain $MgO@SiO_2$ nanocapsules of varying thicknesses. The obtained samples were dried with a rotavapor (Rotavapor R II, BUCHI, Switzerland) at 60 °C and collected for further research.

2.2 Characterization

The elemental composition and site phase composition of the MgO NPs were investigated by X-ray diffraction analysis (XRD, Model D8/Advanced, Bruker, Germany). The diffusion diameters of the samples in ethanol solution were determined by dynamic light scattering (DLS). The zeta potential of the MgO NPs in aqueous solution was measured using a Zetasizer (University of Georgia, Georgia, USA). The overall appearance and morphology of the MgO NPs and $MgO@SiO_2$ nanocapsules, including the thickness of the SiO_2 shell, were characterized by scanning transmission electron microscopy (STEM, University of Georgia, Georgia, USA). The elemental distribution and encapsulation of the silica shell were assessed by energy-dispersive X-ray spectroscopy (EDS, University of Georgia, Georgia, USA).

2.3 Drug release tests

Equal amounts of Mg^{2+} from MgO NPs and $MgO@SiO_2$ nanocapsules were added to 10 mL of deionized water and incubated for 1–5 days. The effect of SiO_2 encapsulation thickness on the degradation of the samples was assessed by measuring the Mg^{2+} content by inductively coupled plasma mass spectrometry (ICP, University of Georgia, Georgia, USA) and plotting the corresponding release curves.

For the control experiments, equal amounts of Mg^{2+} (5 mM) from $MgO@SiO_2$ nanocapsules and MgO NPs were added into 10 mL of deionized water with an initial pH of 7.3 and incubated for 37 °C with gentle shaking for 7 d using an incubator shaker (Marshall Scientific, USA). The pH fluctuations of the mixture were monitored at intervals of 0.5 h, 1 h, 3 h, 6 h, 12 h, 1 d, 2 d, 3 d, 5 d and 7 d. The release of Mg^{2+} from the different samples was evaluated based on the changes in pH value of the solution.

2.4 Cell viability assay

Chondrocytes were isolated and cultured following the methods we previously reported.[23] Briefly, cartilage tissues were isolated from the hip and knee joint of a 10 day-old rat (University of Georgia, Laboratory Animal Center, USA), finely chopped, and rinsed repeatedly with PBS solution. The tissues were digested with 2 mg per mL collagenase II (Solarbio, USA) at 37 °C for 4 h, followed by treatment with 0.25% trypsin/EDTA (Solarbio, USA) at 37 °C for 30 min. The obtained chondrocytes were cultured in culture flasks (37 °C, 5% CO_2, 95% humidity) with 10% (v/v) fetal bovine serum (FBS, Gibco, USA) and 1% (v/v) penicillin/streptomycin in the medium (Gibco, USA). Cells from the second and third passages were used for subsequent experiments.

The chondrocytes were then seeded in 96 well plates at a concentration of 1×10^4 cells per well and incubated for 24 h. The medium was replaced, and different concentrations of MgO NPs and MgO@SiO_2 nanocapsules, $MgCl_2$ and SiO_2 (as control group) were added. After incubation for 24 h, the absorbance of the medium was measured at 570 nm using a plate reader (Biotek Synergy HT, USA) following an MTT assay.

2.5 Animal experiments

This study was approved by the Affiliated Xinhua Hospital of Dalian University Institutional Animal Care and Use Committee (No. 2023-04-01). The animals were provided by the Animal Experiment Center of the Affiliated Xinhua Hospital of Dalian University. Fifteen New Zealand rabbits (2.5–3.0 kg) underwent bilateral anterior cruciate ligament transection (ACLT) and medial meniscectomy operation (MMO) to induce OA. The bilateral knees were shaved and disinfected with an iodine complex prior to surgery. Using an anterior approach to the knee and lateral patellar dislocation, access to the medial compartment of the knee was achieved. The anterior cruciate ligament was carefully severed, and the medial meniscus was completely removed. The joint capsule and skin were sutured and bandaged with sterile dressings.

The rabbits received 1.6 million units of penicillin intramuscularly once a day for 7 days after surgery. They were allowed to eat, drink and move freely in the cages for 4 weeks to develop OA. Next, the animals were randomly assigned to different groups ($n = 3$). The knee joints were injected with 3 mL of either normal saline (control group), $MgCl_2$, MgO NPs, or MgO@SiO_2 with varying shell thicknesses. Intra-articular treatments were initiated 30 days after the OA model induction and were administered every 7 days until the 28th day, for a total of four applications.

2.6 Histological observation

After four weeks of treatment, the animals were anesthetized and sacrificed by exsanguination. The bilateral knee joints were collected and the gross changes in the articular cartilage of the femoral condyles were assessed using the OARSI scoring system,[24] including surface integrity, fissures and erosion. Next, the femoral condyles were fixed in 10% buffered formalin (Beijing Yili, China), decalcified in 10–20% ethylenediaminetetraacetic acid (EDTA, Sigma-Aldrich, USA), and embedded in paraffin. Then, sections were stained with Safranin O-Fast Green Stain Kit (Sigma, USA) according to the manufacturer's instructions. Photographs were taken through an optical microscope (Olympus CKX 41, Japan) to evaluate microscopic cartilage alterations using the OARSI scoring system, including assessments of proteoglycan loss (0–6 points), structural lesions (0–11 points), chondrocyte density (0–4 points) and cluster formation (0–3 points). All scores were independently evaluated by three experienced investigators.

2.7 Immunohistochemical staining

Femoral condyles tissue sections were prepared as described above. First, the sections were deparaffinized and rehydrated through a graded ethanol series. Then, the sections were immersed in a citric acid repair solution (0.01 mol L^{-1}, pH = 6.0) for 5 min, and rinsed with PBS, following which 3% hydrogen peroxide was added and incubated at room temperature for 20 min to quench endogenous peroxidase activity. Next, the samples were blocked with normal goat serum for 30 min and incubated with primary antibodies against IL-1β, P65 and MMP-13 at 4 °C overnight. The next day, the sections were washed three times with PBS and incubated for 20 min with horseradish peroxidase (HRP)-conjugated secondary antibodies (Abcam's 1 : 300–1 : 600 dilution, Ab6789, and 7074, followed by visualization with a Diaminobenzidine (DAB) kit (TA-060-QHDX, Thermo Fisher)). Images of the positive cells and relative intensity were captured using an Olympus photomicroscope (Olympus, Japan).

2.8 Hematologic and biochemical analyses

Blood samples from the rabbit were obtained *via* cephalic or jugular venipuncture prior to sacrifice. Samples for hematologic analyses were collected in tubes containing EDTA (Venosafe Plastic Tubes K2EDTA, Terumo Europe N.V., Leuven, Belgium), while samples for serum biochemical analyses were collected in plain tubes (Venosafe Plastic Tubes with a clot activator, Terumo Europe N.V.). Hematologic analyses were performed within 4 hours of sampling using a Sysmex XN1000 automatic analyzer (Sysmex, Jiangxi, China). Serum biochemical analyses were conducted using a Hitachi 7600 automatic clinical chemistry analyzer (Hitachi Limited, Japan).

2.9 Histopathological examination

The samples of organ tissues, including heart, liver, brain, spleen, lung and kidney, were collected immediately after the animals were sacrificed. All samples were fixed in 10% buffered neutral formalin (Beijing Yili, China). Each specimen was sectioned (5 μm thick), deparaffinized and stained using the hematoxylin–eosin (HE) method. Then, the sections were processed for histopathological assessment and examined under a light microscope at 400× magnification.

2.10 Statistical analysis

Data were processed using GraphPad Prism 9.5 software (Graph Pad, San Diego, CA, USA) and presented as the mean ± SEM.

Statistical analysis was performed using one-way ANOVA, and statistical significance was set at $P < 0.05$.

3 Results and discussion

3.1 MgO@SiO_2 nanocapsule synthesis, characterization and degradation

Firstly, the internal element composition of the synthesized MgO NPs was characterized by X-ray diffraction (XRD), and the results are shown in Fig. 1. Pattern peaks corresponding to the lattice planes (111), (200), (220), (311), and (222) of MgO were identified (Fig. 1a), and Energy Dispersive Spectroscopy (EDS) confirmed that the Mg/O ratio of samples was close to 1 : 1 (Fig. 2b), confirming that MgO was the primary component of the nanoparticles. DLS revealed that the diameter of the MgO nanoparticles was 62.23 ± 10.41 nm in ethanol solution (Fig. 2c). A similar size distribution was observed using STEM, while the nanoparticles were observed to be spherical (Fig. 2a). The size and shape of nanoparticles are well known to be critical factors influencing their cellular uptake mechanisms, biological distribution patterns, and pharmacokinetics.[25] The spherical structure of MgO NPs offers better curvature and is less prone to phagocytosis and cellular internalization compared to nanorods and nanoplates, which helps maintain a consistent concentration within the joint.[26] In additional, the surface potential of nanoparticles is another major factor affecting the stability and properties of nanoparticles, with those having high a negative or positive surface charge being electrostatically repelled and those with a neutral surface being prone to flocculation.[27] In the current study, the average zeta potential of the nanoparticles was +25.99 ± 10.67 V in PBS (Fig. 2d), which makes it easier for the MgO NPs to maintain stability. Our results were also consistent with earlier research, in which the zeta potential value was −15.4 mV, which can effectively stabilize the MgO nanoparticles.[28] Moreover, the positively charged surface is more helpful for the electrostatic adsorption of nanoparticles to articular cartilage, because articular cartilage is often negatively charged.[29] Furthermore, the size of the nanoparticles plays a key role in determining their mode of

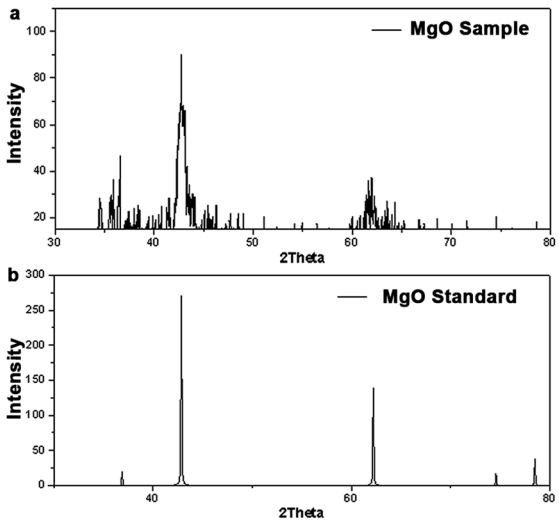

Fig. 1 (a) XRD pattern of the MgO NP sample. (b) XRD pattern of the MgO standard.

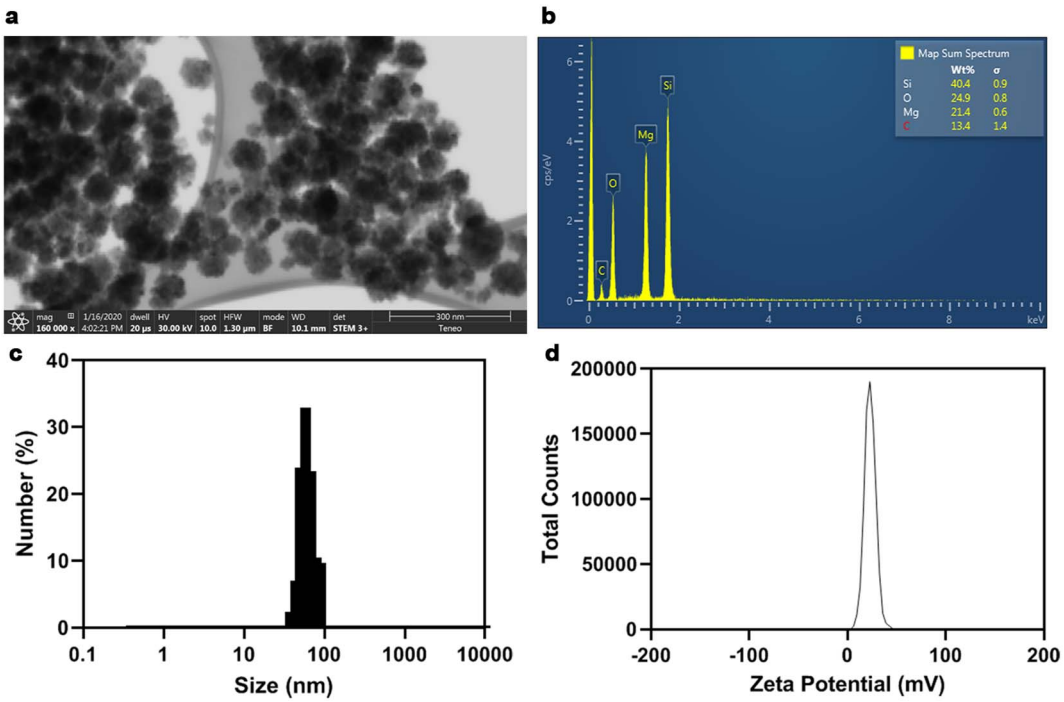

Fig. 2 (a) The shape of MgO nanoparticles using scanning transmission electron microscopy (STEM). (b) Element composition of samples using an energy dispersive spectrum (EDS). (c) DLS of MgO nanoparticles in ethanol. (d) The zeta potential range of MgO nanoparticles in PBS.

endocytosis. Studies have shown that larger particles are internalized through phagocytosis, while smaller nanoparticles are taken up *via* pinocytosis.[30] These distinct endocytosis mechanisms ultimately affect the retention time and ion release rate of nanoparticles, ensuring a more uniform distribution. Our early study results also confirmed that after injecting MgO NPs with different particle sizes into the joint, there were different slow-release Mg^{2+} situations, and samples with larger particle sizes showed a stronger cartilage protection effect.[20] However, we also found that this slow-release effect was relatively weak and can not match the needs of clinical applications.

To slow down the degradation of MgO nanoparticles and improve their ability for sustained release of Mg^{2+}, we coated them with a layer of silica using the Stöber method. Mesoporous silica shells are known for their excellent biocompatibility, low cytotoxicity, and high drug loading capacity and efficiency, making them widely used in cell imaging and drug delivery applications.[31] In the current study, STEM analysis confirmed the formation of a core/shell structure, and EDS further verified that Mg was located in the core, surrounded by a shell of silica (Fig. 3). By varying the amount of tetraethyl orthosilicate (TEOS), we adjusted the silica coating thickness from 30 to 60 nm, which was also confirmed by STEM. These two formulations were referred to as $MgO@SiO_2$30 and $MgO@SiO_2$60, respectively. Previous studies have shown that the dense structure of articular cartilage acts as a barrier to macromolecular drugs and drug delivery systems larger than 100 nm, limiting their effective penetration into deep cartilage and subchondral bone.[32] Therefore, the nanocapsules, being larger than 100 nm, may facilitate early retention in the joint space, enabling the sustained release of magnesium oxide nanoparticles. We subjected the $MgO@SiO_2$ nanocapsules to dialysis in deionized water and quantified magnesium release using Inductively Coupled Plasma Mass Spectrometry (ICP-MS, Fig. 4a). Uncoated MgO NPs released 80% of their total magnesium content within 12 hours of exposure to deionized water. The time required to release 80% of the contained magnesium increased to ~24 hours (81.63% release) with a 30 nm coating, and further extended to ~72 hours (79.27% release) with a 60 nm coating. These results confirmed that silica encapsulation effectively prolongs the release of MgO NPs, with a thicker coating providing a longer release duration. In

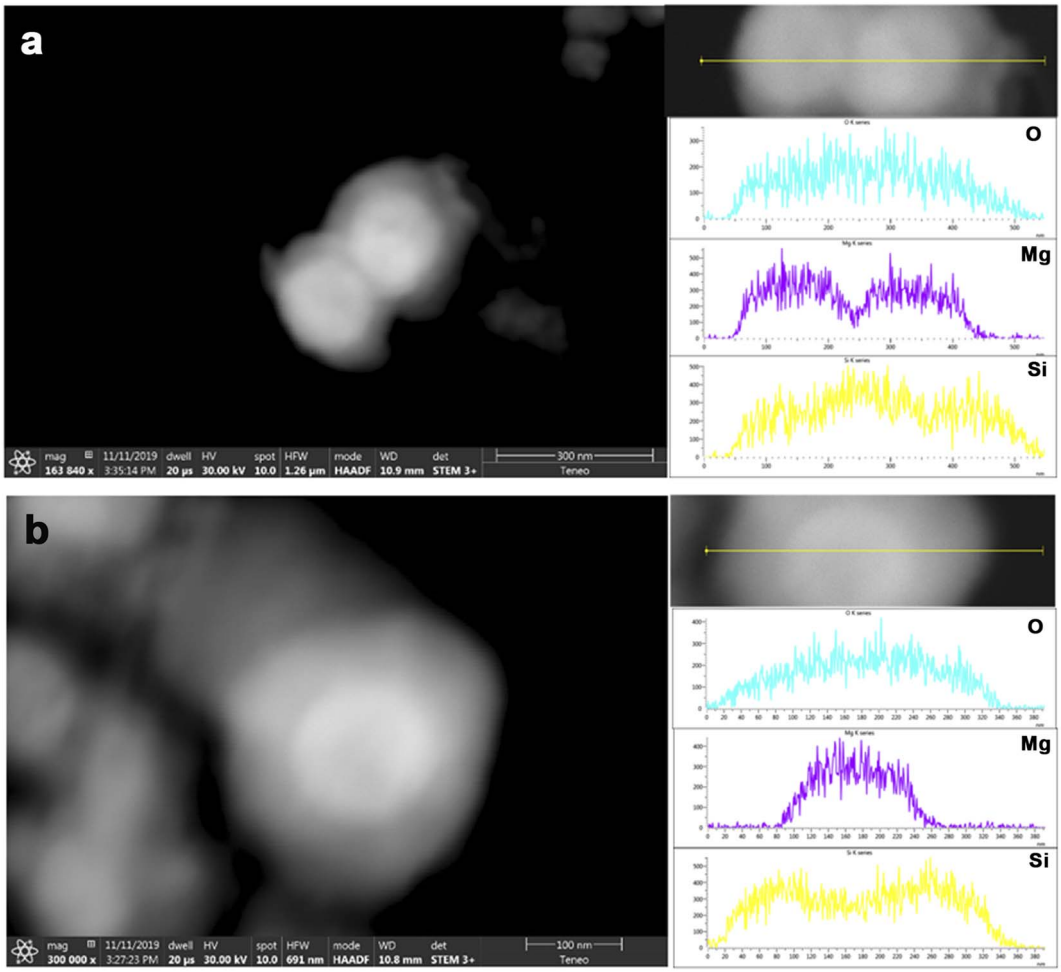

Fig. 3 (a) The shape and element composition of $MgO@SiO_2$30 nanocapsules using scanning transmission electron microscopy (STEM) and an energy dispersive spectrum (EDS). (b) The shape and element composition of $MgO@SiO_2$60 nanocapsules using STEM and EDS.

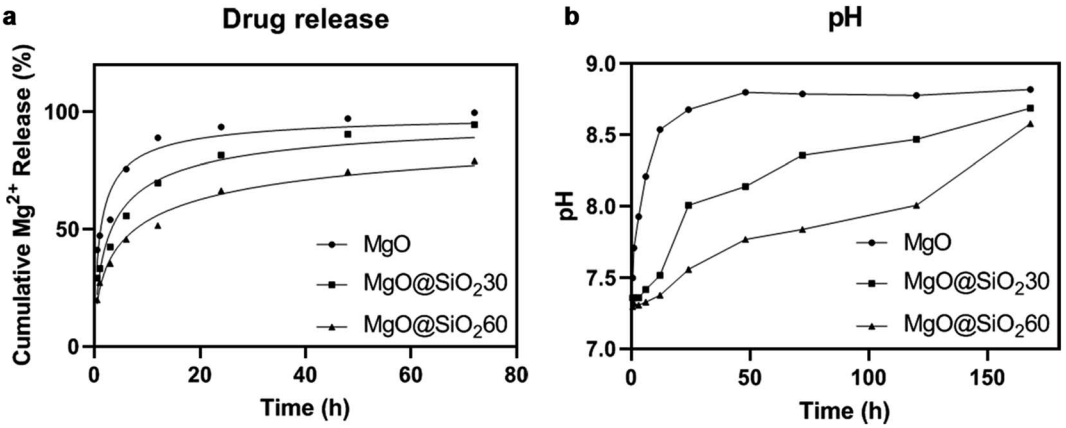

Fig. 4 (a) The released Mg^{2+} fluctuation curve of MgO NPs, MgO@$SiO_2$30 and MgO@$SiO_2$60 nanocapsules (Mg^{2+}, 5 mM) monitored by ICP-MS at different times in 10 mL deionized water. (b) The pH value fluctuation curve of MgO NPs, MgO@$SiO_2$30 and MgO@$SiO_2$60 nanocapsules monitored during immersing for 1 week in 10 mL deionized water.

addition, the degradation behavior and Mg^{2+} release was evaluated indirectly by monitoring the pH variation in water. The degradation reaction for MgO-based materials can be represented as follows: $MgO + H_2O \rightarrow Mg^{2+} + 2OH^-$. This indicates that the generation of 1 mol of Mg^{2+} consumes 1 mol of MgO while producing 2 mol of OH^-. In this study, the MgO group exhibited more significant pH value changes than all other groups, particularly during the initial 12 h (Fig. 4b). In contrast, the pH value of the MgO@SiO_2 groups increased steadily and slowly in 72 h; more importantly, we found that with the increase of thickness of SiO_2 cladding, the rising trend of pH decreased, indicating SiO_2 can effectively prevent MgO degradation.

3.2 MgO@SiO_2 nanocapsule cytotoxicity, efficacy and biosafety

Next, we evaluated the cytotoxicity of MgO@SiO_2 nanocapsules on articular chondrocytes isolated from rat knee joints using an MTT assay. In a normal culture medium, chondrocyte viability was 82% and 75% for magnesium chloride ($MgCl_2$) and silicon dioxide (SiO_2) at a concentration of 5 mM (Fig. 5). Meanwhile, levels of chondrocyte viability of MgO NPs, MgO@$SiO_2$30, and MgO@$SiO_2$60 nanocapsules were 72%, 71% and 74%, respectively. In contrast to the comparable levels of chondrocyte viability at 5 mM, the levels of MgO@$SiO_2$30 and MgO@$SiO_2$60 nanocapsules increased to 80% and 79% at 2.5 mM, while the levels of MgO NPs and SiO_2 groups were stable at 71% and 73%. Note that according to the ISO 10993 standard, samples with cell viability below 70% are considered cytotoxic.[33] Although the viability of all samples was more than 70% at both 5 mM and 2.5 mM concentrations, for safety purposes we used a maximum concentration of 2.5 mM MgO@SiO_2 nanocapsules in subsequent experiments.

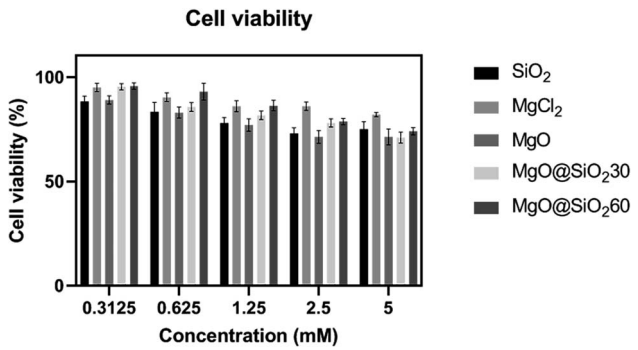

Fig. 5 Cell viability evaluation by the CCK-8 assay after treatment with MgO NPs, MgO@$SiO_2$30 and MgO@$SiO_2$60 nanocapsules on viability and proliferation of chondrocytes.

The efficacy of MgO@SiO_2 nanocapsules was further evaluated in a New Zealand rabbit OA model that had undergone bilateral anterior cruciate ligament transection (ACLT) and medial meniscectomy operation (MMO) surgery. One month after the surgical procedure to induce OA, the animals were randomly assigned to four groups ($n = 12$) and received weekly intra-articular (i.a.) injections of 1.5 mL of either $MgCl_2$ salt, MgO NPs, MgO@$SiO_2$30, or MgO@$SiO_2$60 nanocapsules, all at a magnesium concentration of 2.5 mM. A total of four injections were administered, and the animals were euthanized after 4 weeks. Medical saline (NaCl) was used as a control throughout the experiment, and no signs of acute inflammation were observed in any of the treatment groups. In the NaCl-treated group, characteristic OA features such as erosion, osteophyte formation, and large areas of lesions were evident (Fig. 6a). Treatment with $MgCl_2$ led to moderate OA regression, consistent with previous observations.[34] In comparison, the groups treated with MgO NPs showed significantly reduced cartilage damage, likely due to the slower clearance of nanoparticles compared to Mg salts. Early studies have also shown that MgO NPs not only could promote the differentiation of chondrocytes and inhibit the destruction of the extracellular matrix (ECM) by releasing magnesium ions,[35–37] but also played an anti-ROS role to reduce the inflammatory response in local cartilage tissue,[38,39] thus playing an anti-OA role. The OARSI scores for the general appearance of cartilage were also evaluated, with the

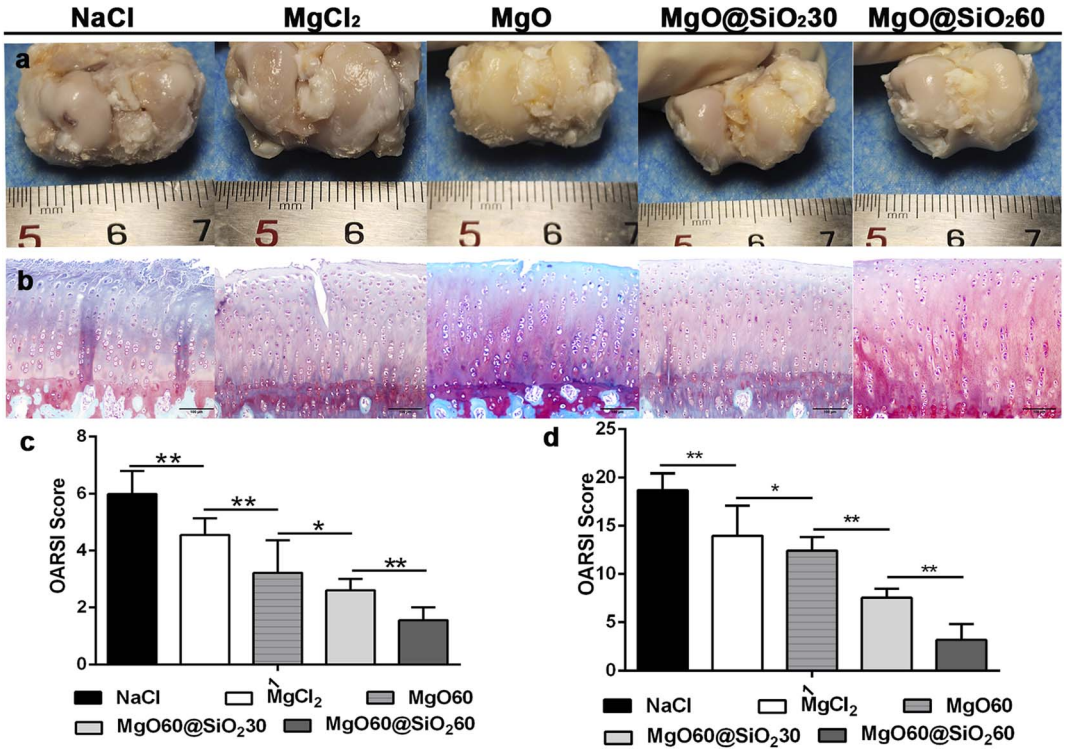

Fig. 6 Representative photographs showing the macroscopic and histology appearance of the cartilage from the femoral condyles after treatment for 4 weeks. (a) General appearance, (b) safranin O-fast green staining, (c) macroscopic evaluations of cartilage changes after treatments according to the OARSI standard ($p < 0.05$). (d) Microscopic OARSI scores of articular cartilage changes ($p < 0.05$).

NaCl group scoring 6.33 ± 0.33 and the $MgCl_2$ group scoring 4.56 ± 0.41. After nanoparticle treatment, the OARSI scores decreased to 3.56 ± 0.67, 2.61 ± 0.3, and 1.22 ± 0.22, for the MgO, MgO@$SiO_2$30, and MgO@$SiO_2$60 groups, aligning with the general appearance results (Fig. 6c). In our study, the MgO@$SiO_2$30 and MgO@$SiO_2$60 groups demonstrated better preservation of articular cartilage structure, presumably due to the prolonged Mg release and extended action time provided by the silica-coated formulations.

Next, in order to further verify that SiO_2 sustained-release MgO NPs can help to combat the pathological process of OA, the histological analysis of cartilage changes was conducted using safranin O-fast green staining (Fig. 6b and d). Typical OA features, such as fibrillated lesions, chondrocyte clusters, and loss of GAG, were observed in the NaCl group. Compared to the NaCl control, all treatment groups showed varying degrees of improvement in morphological changes, proteoglycan retention, and tidemark integrity. Among the treatments, MgO@$SiO_2$60 was the most effective in maintaining the normal columnar architecture of cartilage, as evidenced by less severe lesions on the condyle surface, decreased fibrillation/fissures, and increased tissue cellularity and cloning (Fig. 6b). Additionally, the MgO@$SiO_2$60 group exhibited more intense safranin O-fast green positive staining than the control groups. The OARSI histological scores were consistent with these findings (Fig. 6d). Specifically, the scores were 18.72 ± 1.3 and 14 ± 2.44 for the NaCl and $MgCl_2$ groups, respectively, while the MgO NPs and MgO@$SiO_2$30 groups scored 12.44 ± 1.04 and 7.56 ± 0.74. The MgO@$SiO_2$60 group achieved a favorable OARSI histological score of 3.17 ± 1.22. These results are also similar to the general appearance, which fully indicates that sustained release of MgO and Mg^{2+} is closely related to the injury degree of OA cartilage tissue.

Finally, we assessed the bio-safety of MgO@SiO_2 nanocapsules using hematologic and histopathological methods. Hematologic and serum biochemical indices, including WBC, RBC, hemoglobin (HGB), hematocrit (HCT), glutamic-pyruvic transaminase (ALT), glutamic-oxaloacetic transaminase (AST), alkaline phosphatase (ALP), creatinine (CREA), blood urea nitrogen (BUN), Na^+, K^+, Mg^{2+}, and Ca^{2+}, were examined and are presented in Table 1. Histopathological sections from major organs, including the heart, liver, brain, spleen, lung, and kidney, were stained using the H&E method to assess cell structure and morphology (Fig. 8). Our results indicated that all hematologic and biochemical indices remained stable throughout the experiment, and no significant abnormalities were observed in the pathology of major organs. Overall, MgO@SiO_2 nanocapsules appear to be safe for administration *via* intra-articular injection.

3.3 Mechanism of MgO@SiO_2 nanocapsules for treatment of OA

To further explore the potential mechanism of MgO@SiO_2 nanocapsules in the treatment of OA, we also assessed the impact of samples on OA-related catabolic markers. As is well

Table 1 Effect of MgO@SiO_2 nanocapsules on hematologic and serum biochemical analyses[a]

	NaCl	$MgCl_2$	MgO NPs	MgO/$SiO_2$30	MgO/$SiO_2$60	*P* value
WBC	7.98 ± 1.61	7.39 ± 1.14	7.90 ± 2.30	8.06 ± 2.45	7.99 ± 0.59	0.99
RBC	6.19 ± 1.48	6.21 ± 0.45	5.87 ± 0.48	6.02 ± 0.57	6.25 ± 1.82	0.992
HGB	119.33 ± 29.26	117 ± 4.00	109.33 ± 7.57	114.33 ± 15.7	118.67 ± 28.54	0.97
HCT	39.63 ± 6.34	38.83 ± 1.25	35.27 ± 2.15	37.93 ± 2.66	33 ± 13.29	0.742
ALT	37.13 ± 11.00	35.67 ± 17.98	37.23 ± 5.48	39.67 ± 6.22	40.37 ± 11.29	0.984
AST	28.27 ± 5.44	25.93 ± 13.37	19.17 ± 3.52	25.1 ± 12.62	28.47 ± 5.90	0.727
ALP	80.03 ± 23.55	76.43 ± 1.94	56.77 ± 48.49	41.33 ± 21.85	43.67 ± 43.26	0.484
CREA	86.33 ± 21.55	97 ± 14.73	82.33 ± 16.5	81.00 ± 11.79	86.67 ± 37.07	0.909
BUN	6.33 ± 0.98	8.43 ± 2.48	5.8 ± 1.13	6.77 ± 2.23	7.57 ± 2.05	0.489
Na^+	144.33 ± 2.76	142.5 ± 3.75	142.67 ± 1.55	142.17 ± 3.18	142.67 ± 0.15	0.863
K^+	7.99 ± 0.38	6.5 ± 0.43	6.54 ± 0.56	6.39 ± 0.56	6.65 ± 1.11	0.901
Ca^{2+}	3.71 ± 0.10	3.68 ± 0.24	3.38 ± 0.45	3.62 ± 0.10	3.41 ± 0.20	0.413
Mg^{2+}	1.09 ± 0.17	1.17 ± 0.29	1.06 ± 0.27	1.1 ± 0.02	1.09 ± 0.25	0.999

[a] HGB: hemoglobin; HCT: hematocrit; ALT: glutamic-pyruvic transaminase; AST: glutamic-oxaloacetic transaminase; ALP: alkaline phosphatase; CREA: creatinine; BUN: blood urea nitrogen.

known, OA results from the failure of the repair process of damaged cartilage by aseptic inflammation caused by biomechanical and biochemical changes in the joints. Therefore, inflammatory cytokines play a crucial role in the pathological process of OA. IL-1β is currently recognized as one of the most important cytokines in the OA inflammatory response. It is synthesized locally by synoviocytes and chondrocytes[40] and can enhance the expression of NF-κB/p65, thereby activating the NF-κB/p65 signaling pathway, which is proinflammatory.[41] Meanwhile, excessive activation of p65 and subsequent transactivation of effector molecules play a crucial role in the pathogenesis of many chronic diseases,[42] including OA.[43] In addition, MMP-13 is a central node in the cartilage degradation network, being significantly overexpressed in the joints and articular cartilage of patients with OA, while being scarcely detected in normal adult tissues.[44] Therefore, the MMP-13 levels correlate with the presence of pathological chondrocytes undergoing hypertrophic differentiation in the early stages of OA development,[45] and its overexpression can induce OA through excessive ECM degradation.[46]

In the current study, we observed significant increases in IL-1β, p65 and MMP13 expression in the NaCl-treated group (Fig. 7), which fully confirmed that the NF-κB/p65 signaling pathway was activated to induce inflammation, causing injury and degeneration of cartilage in knee joint of rabbits undergoing ACLT + MMO surgery. Moreover, our analysis showed that $MgCl_2$ treatment inhibited IL-1β, p65, and MMP-13 levels in OA cartilage compared to NaCl alone, which suggests that magnesium supplementation in the joint can reduce inflammatory response.[12,46] More importantly even greater suppression of these markers was observed in the groups treated with MgO NPs, MgO@$SiO_2$30, and MgO@$SiO_2$60, with MgO@$SiO_2$60 demonstrating the most significant inhibition, suggesting that inflammation in OA cartilage was sustainably relieved with

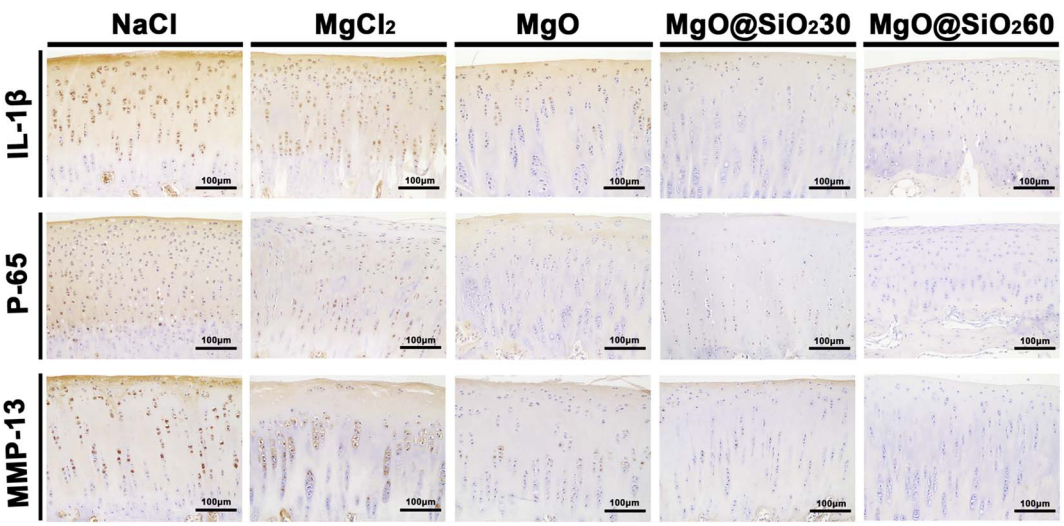

Fig. 7 The image of immunohistochemical staining on OA-related catabolic markers, including IL-1β, NF-κB/p65, and MMP13 expression after treatment with NaCl, $MgCl_2$, MgO NPs, MgO@$SiO_2$30 and MgO@$SiO_2$60 nanocapsules.

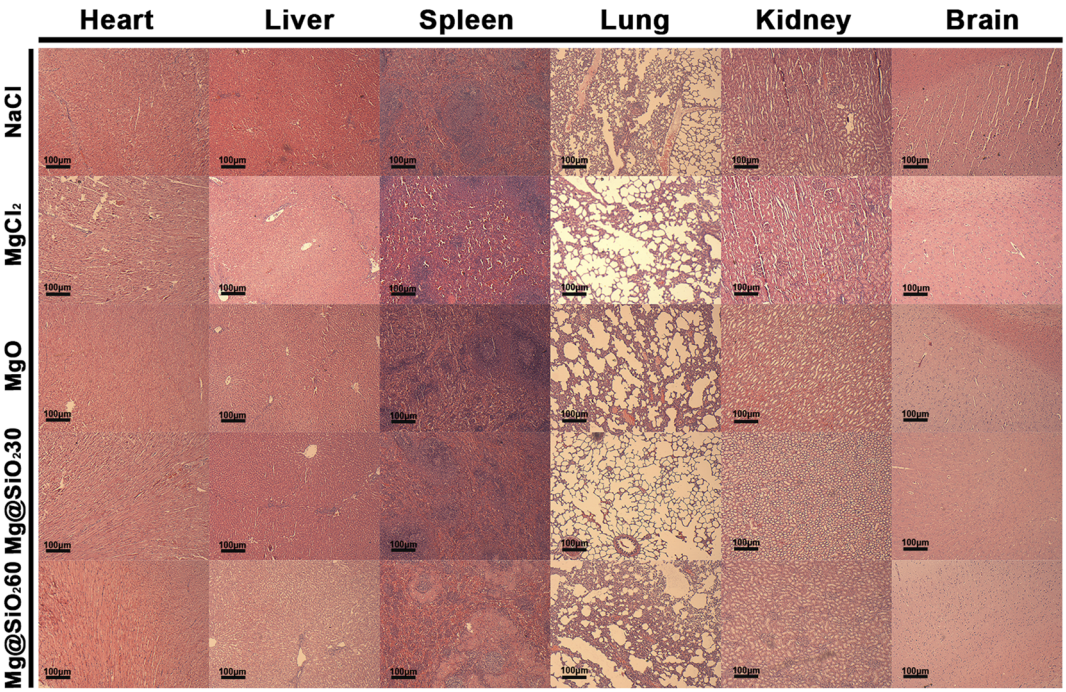

Fig. 8 H&E staining images of organ histological evaluation, including heart, liver, spleen, lung, kidney and brain treated with NaCl (normal saline), $MgCl_2$, MgO NPs, MgO@$SiO_2$30 and MgO@$SiO_2$60 nanocapsules after 4 weeks.

continuous release of magnesium ions. Combined with the gross appearance and histological results described above, our results suggest that Mg nanoparticles exert their effects by inhibiting IL-1β expression and blocking the NF-κB/p65 pathway. The silica coating likely contributes to the enhanced suppressive effects by enabling the sustained release of magnesium ions.

There are several limitations to the current study. First, the potential cross-reactions between the nanoparticles themselves and articular cartilage or cells have not been studied in depth, which could lead to potential risks when used clinically. Second, the release of MgO NPs and Mg^{2+} in the MgO@SiO_2 nanocapsules in articular cartilage was not clearly measured, which needs further study to clarify. At last, it will also be important to understand the metabolism behavior of MgO and magnesium ions in joints. These investigations are underway.

4 Conclusion

In this study, we developed an innovative magnesium ion delivery system to achieve controlled release of Mg^2 in the joint space, which will help further clarify the promotion and application of nanocapsule technology in the field of OA therapy. Using the Stöber method, we encapsulated MgO nanoparticles within a SiO_2 capsule, with the core/shell structure verified by microscopic and elemental analysis. The MgO@SiO_2 nanocapsules enhanced the bioavailability of Mg^{2+}, resulting in significantly improved moderation of OA progression and effective cartilage protection. These nanocapsules also demonstrated excellent biosafety throughout the experiments. The inhibition of OA progression is likely due to the sustained release of Mg^{2+} from the nanocapsules, which reduces the production of inflammatory factors associated with the NF-κB/p65 pathway. Overall, this study represents a novel approach for effective and low-toxicity OA treatment with significant potential for clinical application, which is helpful to solve the problem of expanding the production scale of nanocapsules. This method can be extended to the controlled release of other electrolytes for broader applications.

Consent for publication

All authors have read and approved the manuscript.

Ethical statement

All animal experiments were approved by the Animal Care and Use Committee of Affiliated Xinhua Hospital of Dalian University (No. 2023-04-01), and were performed in compliance with the relevant local guidelines and the Declaration of Helsinki.

Data availability

The data supporting this article have been included as part of the ESI.†

Author contributions

Na Liu and Fangchao Jiang wrote the original manuscript text and prepared Fig. 1–3; Zhizi Feng: statistics and image editing; Wei Yang and Weizhong Zhang prepared Fig. 4 and 5; Na Liu and Sen Mei prepared Fig. 6; Yu Zheng and Benjie Wang

prepared Fig. 7; Yingna Cui prepared Fig. 8; Jin Xie and Nan Zhang wrote, reviewed and edited the main manuscript text.

Conflicts of interest

All authors declared that no conflict of interest exists in the submission of this manuscript.

Acknowledgements

This work was financially supported by funds from the Interdisciplinary Project of Dalian University (DLUXK-2023-YB-008) and Key Discipline Project of Affiliated Xinhua Hospital of Dalian University (2022003).

References

1 M. C. C. Minnig, Y. M. Golightly and A. E. Nelson, Epidemiology of osteoarthritis: literature update 2022-2023, *Curr. Opin. Rheumatol.*, 2024, **36**(2), 108–112.
2 J. N. Katz, K. R. Arant and R. F. Loeser, Diagnosis and Treatment of Hip and Knee Osteoarthritis: A Review, *J. Am. Med. Assoc.*, 2021, **325**(6), 568–578.
3 F. Motta, E. Barone, A. Sica and C. Selmi, Inflammaging and Osteoarthritis, *Clin. Rev. Allergy Immunol.*, 2023, **64**(2), 222–238.
4 B. F. Ricciardi, G. Muthukrishnan, E. A. Masters, N. Kaplan, J. L. Daiss and E. M. Schwarz, New developments and future challenges in prevention, diagnosis, and treatment of prosthetic joint infection, *J. Orthop. Res.*, 2020, **38**(7), 1423–1435.
5 H. Yao, J. Xu, J. Wang, Y. Zhang, N. Zheng, J. Yue, J. Mi, L. Zheng, B. Dai, W. Huang, S. Yung, P. Hu, Y. Ruan, Q. Xue, K. Ho and L. Qin, Combination of magnesium ions and vitamin C alleviates synovitis and osteophyte formation in osteoarthritis of mice, *Bioact. Mater.*, 2020, **6**(5), 1341–1352.
6 X. Kuang, J. Chiou, K. Lo and C. Wen, Magnesium in joint health and osteoarthritis, *Nutr. Res.*, 2021, **90**, 24–35.
7 A. H. Martinez Sanchez, F. Feyerabend, D. Laipple, R. Willumeit-Römer, A. Weinberg and B. J. C. Luthringer, Chondrogenic differentiation of ATDC5-cells under the influence of Mg and Mg alloy degradation, *Mater. Sci. Eng., C*, 2017, **72**, 378–388.
8 M. Shimaya, T. Muneta, S. Ichinose, K. Tsuji and I. Sekiya, Magnesium enhances adherence and cartilage formation of synovial mesenchymal stem cells through integrins, *Osteoarthr. Cartil.*, 2010, **18**(10), 1300–1309.
9 F. Feyerabend, F. Witte, M. Kammal and R. Willumeit, Unphysiologically high magnesium concentrations support chondrocyte proliferation and redifferentiation, *Tissue Eng.*, 2006, **12**(12), 3545–3556.
10 N. Zhang, W. Wang, X. Zhang, K. C. Nune, Y. Zhao, N. Liu, R. D. K. Misra, K. Yang, L. Tan and J. Yan, The effect of different coatings on bone response and degradation behavior of porous magnesium-strontium devices in segmental defect regeneration, *Bioact. Mater.*, 2020, **6**(6), 1765–1776.
11 Y. Li, J. Yue and C. Yang, Unraveling the role of Mg(++) in osteoarthritis, *Life Sci.*, 2016, **147**, 24–29.
12 H. Yao, J. K. Xu, N. Y. Zheng, J. L. Wang, S. W. Mok, Y. W. Lee, L. Shi, J. Y. Wang, J. Yue, S. H. Yung, P. J. Hu, Y. C. Ruan, Y. F. Zhang, K. W. Ho and L. Qin, Intra-articular injection of magnesium chloride attenuates osteoarthritis progression in rats, *Osteoarthr. Cartil.*, 2019, **27**(12), 1811–1821.
13 C. H. Evans, V. B. Kraus and L. A. Setton, Progress in intra-articular therapy, *Nat. Rev. Rheumatol.*, 2014, **10**(1), 11–22.
14 G. Z. Jin, Current Nanoparticle-Based Technologies for Osteoarthritis Therapy, *Nanomaterials*, 2020, **10**(12), 2368.
15 M. A. Ammulu, K. Vinay Viswanath, A. K. Giduturi, P. K. Vemuri, U. Mangamuri and S. Poda, Phytoassisted synthesis of magnesium oxide nanoparticles from Pterocarpus marsupium rox.b heartwood extract and its biomedical applications, *J. Genet. Eng. Biotechnol.*, 2021, **19**(1), 21.
16 M. A. Ammulu, K. Vinay Viswanath, A. K. Giduturi, P. K. Vemuri, U. Mangamuri and S. Poda, Phytoassisted synthesis of magnesium oxide nanoparticles from Pterocarpus marsupium rox.b heartwood extract and its biomedical applications, *J. Genet. Eng. Biotechnol.*, 2021, **19**(1), 21.
17 A. Mahmoud, Ö. Ezgi, A. Merve and G. Özhan, In Vitro Toxicological Assessment of Magnesium Oxide Nanoparticle Exposure in Several Mammalian Cell Types, *Int. J. Toxicol.*, 2016, **35**(4), 429–437.
18 Y. Chen, W. Sheng, J. Lin, C. Fang, J. Deng, P. Zhang, M. Zhou, P. Liu, J. Weng, F. Yu, D. Wang, B. Kang and H. Zeng, Magnesium Oxide Nanoparticle Coordinated Phosphate-Functionalized Chitosan Injectable Hydrogel for Osteogenesis and Angiogenesis in Bone Regeneration, *ACS Appl. Mater. Interfaces*, 2022, **14**(6), 7592–7608.
19 L. Zheng, S. Zhao, Y. Li, J. Xu, W. Yan, B. Guo, J. Xu, L. Jiang, Y. Zhang, H. Wei and Q. Jiang, Engineered MgO nanoparticles for cartilage-bone synergistic therapy, *Sci. Adv.*, 2024, **10**(10), eadk6084.
20 S. Mei, F. Jiang, N. Liu, Z. Feng, Y. Zheng, W. Yang, W. Zhang, Y. Cui, W. Wang, J. Xie and N. Zhang, Sol-gel synthesis of magnesium oxide nanoparticles and their evaluation as a therapeutic agent for the treatment of osteoarthritis, *Nanomedicine*, 2024, **19**(23), 1867–1878.
21 N. Mazaheri, N. Naghsh, A. Karimi and H. Salavati, In vivo Toxicity Investigation of Magnesium Oxide Nanoparticles in Rat for Environmental and Biomedical Applications, *Iran. J. Biotechnol.*, 2019, **17**(1), e1543.
22 Z. Liu, Z. Yin, C. Cox, M. Bosman, X. Qian, N. Li, H. Zhao, Y. Du, J. Li and D. G. Nocera, Room temperature stable COx -free H2 production from methanol with magnesium oxide nanophotocatalysts, *Sci. Adv.*, 2016, **2**(9), e1501425.
23 T. Todd, Z. Lu, J. Zhao, B. Cline, W. Zhang, H. Chen, A. Kumar, W. Jiang, F. West, S. Franklin, L. Zheng and J. Xi, LiF@SiO2 nanocapsules for controlled lithium

release and osteoarthritis treatment, *Nano Res.*, 2018, **11**(10), 5751–5760.

24 S. Laverty, C. A. Girard, J. M. Williams, E. B. Hunziker and K. P. Pritzker, The OARSI histopathology initiative - recommendations for histological assessments of osteoarthritis in the rabbit, *Osteoarthr. Cartil.*, 2010, **18**(suppl. 3), S53–S65.

25 C. Kinnear, T. L. Moore, L. Rodriguez-Lorenzo, B. Rothen-Rutishauser and A. Petri-Fink, Form Follows Function: Nanoparticle Shape and Its Implications for Nanomedicine, *Chem. Rev.*, 2017, **117**(17), 11476–11521.

26 S. Podder, D. Chanda, A. K. Mukhopadhyay, A. De, B. Das, A. Samanta, J. G. Hardy and C. K. Ghosh, Effect of Morphology and Concentration on Crossover between Antioxidant and Pro-oxidant Activity of MgO Nanostructures, *Inorg. Chem.*, 2018, **57**(20), 12727–12739.

27 N. T. T. Nguyen, L. M. Nguyen, T. T. T. Nguyen, U. P. N. Tran, D. T. C. Nguyen and T. V. Tran, A critical review on the bio-mediated green synthesis and multiple applications of magnesium oxide nanoparticles, *Chemosphere*, 2023, **312**(pt 1), 137301.

28 J. Jeevanandam, Y. S. Chan and M. K. Danquah, Cytotoxicity and insulin resistance reversal ability of biofunctional phytosynthesized MgO nanoparticles, *3 Biotech.*, 2020, **10**(11), 489.

29 K. Bhardwaj, D. S. Dhanjal, A. Sharma, E. Nepovimova, A. Kalia, S. Thakur, S. Bhardwaj, C. Chopra, R. Singh, R. Verma, D. Kumar, P. Bhardwaj and K. Kuča, Conifer-Derived Metallic Nanoparticles: Green Synthesis and Biological Applications, *Int. J. Mol. Sci.*, 2020, **21**(23), 9028.

30 H. Hadji and K. Bouchemal, Effect of micro- and nanoparticle shape on biological processes, *J. Controlled Release*, 2022, **342**, 93–110.

31 Y. Chen, H. Chen, D. Zeng, Y. Tian, F. Chen, J. Feng and J. Shi, Core/shell structured hollow mesoporous nanocapsules: a potential platform for simultaneous cell imaging and anticancer drug delivery, *ACS Nano*, 2010, **4**(10), 6001–6013.

32 T. K. Mwangi, I. M. Berke, E. H. Nieves, R. D. Bell, S. B. Adams and L. A. Setton, Intra-articular clearance of labeled dextrans from naive and arthritic rat knee joints, *J. Controlled Release*, 2018, **283**, 76–83.

33 C. C. Coelho, R. Araújo, P. A. Quadros, S. R. Sousa and F. J. Monteiro, Antibacterial bone substitute of hydroxyapatite and magnesium oxide to prevent dental and orthopaedic infections, *Mater. Sci. Eng., C*, 2019, **97**, 529–538.

34 X. Kuang, J. Chiou, K. Lo and C. Wen, Magnesium in joint health and osteoarthritis, *Nutr. Res.*, 2021, **90**, 24–35.

35 Y. Dou, N. Li, Y. Zheng and Z. Ge, Effects of fluctuant magnesium concentration on phenotype of the primary chondrocytes, *J. Biomed. Mater. Res., Part A*, 2014, **102**(12), 4455–4463.

36 S. Li, F. Ma, X. Pang, B. Tang and L. Lin, Synthesis of chondroitin sulfate magnesium for osteoarthritis treatment, *Carbohydr. Polym.*, 2019, **212**, 387–394.

37 J. Yue, S. Jin, S. Gu, R. Sun and Q. Liang, High concentration magnesium inhibits extracellular matrix calcification and protects articular cartilage via Erk/autophagy pathway, *J. Cell. Physiol.*, 2019, **234**(12), 23190–23201.

38 S. Shankar, A. N. Murthy, P. Rachitha, V. B. Raghavendra, N. Sunayana, A. Chinnathambi, S. A. Alharbi, N. Basavegowda, K. Brindhadevi and A. Pugazhendhi, Silk sericin conjugated magnesium oxide nanoparticles for its antioxidant, anti-aging, and anti-biofilm activities, *Environ. Res.*, 2023, **223**, 115421.

39 Y. Chen, W. Sheng, J. Lin, C. Fang, J. Deng, P. Zhang, M. Zhou, P. Liu, J. Weng, F. Yu, D. Wang, B. Kang and H. Zeng, Magnesium Oxide Nanoparticle Coordinated Phosphate-Functionalized Chitosan Injectable Hydrogel for Osteogenesis and Angiogenesis in Bone Regeneration, *ACS Appl. Mater. Interfaces*, 2022, **14**(6), 7592–7608.

40 M. Husa, F. Petursson, M. Lotz, R. Terkeltaub and R. Liu-Bryan, C/EBP homologous protein drives pro-catabolic responses in chondrocytes, *Arthritis Res. Ther.*, 2013, **15**(6), R218.

41 T. Lawrence, The nuclear factor NF-kappa B pathway in inflammation, *Cold Spring Harbor Perspect. Biol.*, 2009, **1**(6), a001651.

42 H. Mao, B. Han, H. Li, Y. Tao and W. Wu, FABP4 knockdown suppresses inflammation, apoptosis and extracellular matrix degradation in IL-1β-induced chondrocytes by activating PPARγ to regulate the NF-κB signaling pathway, *Mol. Med. Rep.*, 2021, **24**(6), 855.

43 S. Giridharan and M. Srinivasan, Mechanisms of NF-κB p65 and strategies for therapeutic manipulation, *J. Inflammation Res.*, 2018, **11**, 407–419.

44 H. Li, D. Wang, Y. Yuan and J. Min, New insights on the MMP-13 regulatory network in the pathogenesis of early osteoarthritis, *Arthritis Res. Ther.*, 2017, **19**(1), 248.

45 S. Kamekura, K. Hoshi, T. Shimoaka, U. Chung, H. Chikuda, T. Yamada, M. Uchida, N. Ogata, A. Seichi, K. Nakamura and H. Kawaguchi, Osteoarthritis development in novel experimental mouse models induced by knee joint instability, *Osteoarthr. Cartil.*, 2005, **13**(7), 632–641.

46 M. Nugent, MicroRNAs: exploring new horizons in osteoarthritis, *Osteoarthr. Cartil.*, 2016, **24**(4), 573–580.